Nature of the Crystalline Interphase in Sheared IPP/Vectra Fiber Model Composites by Microfocus X-ray Diffraction and IR Microspectroscopy Using Synchrotron Radiation

Javier Torre and Milagros Cortázar

Departamento de Ciencia y Tecnología de Polímeros, Facultad de Química, Universidad del País Vasco (UPV/EHU), Apartado 1072, 20080 San Sebastián, Spain

Marian A. Gómez, Carlos Marco, and Gary Ellis*

Departamento de Física e Ingeniería de Polímeros, Instituto de Ciencia y Tecnología de Polímeros (CSIC), Juan de la Cierva 3, 28006 Madrid, Spain

Christian Riekel

European Synchrotron Radiation Facility, B.P. 220, F-38043 Grenoble Cedex, France

Paul Dumas

Synchrotron SOLEIL, L'Orme des Merisiers, Saint-Aubin, B.P. 48, 91192 Gif-sur-Yvette Cedex, France

Received April 4, 2006
Revised Manuscript Received June 19, 2006

Introduction

Fiber-reinforced crystallizable thermoplastic polymers draw considerable attention in the literature because of their fundamental importance in the development of composite materials with attractive thermal and mechanical properties. It is well-known that the presence of reinforcing fibers can significantly modify the crystallization behavior from the quiescent melt of semicrystalline polymers such as polypropylene,[1−4] their surfaces providing heterogeneous nucleating sites. When a high nucleation density is obtained at the fiber surface, the habitual three-dimensional spherulitic growth is impeded due to overcrowding by neighboring entities, such that the resulting crystalline growth front is perpendicular to the fiber surface, and the so-called *transcrystalline* morphology is formed around the fiber. Since the first observation of transcrystallinity,[5] the nature of this phenomenon has been extensively studied and recently reviewed.[6]

Isotactic polypropylene, iPP, exhibits three crystalline polymorphs, α, β, and γ, and a metastable *smectic* form, whose formation depends on the crystallization conditions.[7−12] The monoclinic α-modification predominates because it is thermodynamically more stable when melt-processed under normal conditions, and a spherulitic morphology is usually observed. Correspondingly, in the vast majority of systems where fiber-reinforcement generates a transcrystalline morphology, the α-form is observed in the transcrystalline region. The nucleating ability of many different types of fibers has been reported such as glass,[13−18] carbon,[19−23] and vegetable fibers[24−26] as well as some polymeric fibers,[6,17,20,24,27] including LCP fibers.[28−30] Only a few fibers have been reported to generate a transcrystalline β-phase in iPP from a quiescent melt, such as bamboo fibers,[25] glass, or polymer fibers coated with β-nucleating agents,[42−44] and more recently, single-polymer fiber−matrix homogeneity composites.[45,46] A precise description of the mechanisms involved in the generation of the β-phase is still a much debated issue.

Recently, significant interest has centered on the trigonal β-modification because a high proportion of the β-phase can lead to improved mechanical properties, particularly toughness and impact strength.[31−34] However, crystallization of the lower stability β-modification requires specific conditions such as thermal gradients[35] or shear stresses,[19,36] or the presence of low concentrations of selective β nucleating agents.[34,37−40] In the latter case, by far the most widely studied, the resulting β-rich iPP generally contains a varying amount of the α-modification which will depend on the efficiency of the nucleation agent,[11,41] although pure β-iPP has been reported.[38,39] It should also be pointed out that structures rich in the β-modification form if the crystallization takes place in the temperature range of 100−141 °C.[19,34]

β-phase transcrystalline-like morphologies can also be generated by the application of shear stress,[13−16,19,23,47,48] for example, by pulling the fiber in the crystallizing polymer melt. The shear at the polymeric matrix−fiber interface leads to specific alignments of the macromolecular chains in the vicinity of fiber. The morphology developed during the crystallization process is termed *cylindritic*,[19,41] differentiating it from transcrystalline superstructures because the crystallization is induced by self-nucleation of the polymeric matrix rather than heterogeneous nucleation on a foreign surface. Thus the nature of the fiber is less important, and even fibers without nucleating ability can generate self-nucleation sites in iPP when pulled through the crystallizing melt.

Currently accepted models to explain the origin of the β-cylindritic phase are based on the careful and systematic work of Varga and Karger-Kocsis in pulled-fiber systems.[15,16,19,23,47] They proposed that the shear produced in the melt by fiber-pulling generated a series of α-row nuclei along the surface of the fiber.[19] At the interface of this thin layer of oriented α-crystals, a transition from the α- to the β-phase takes place, termed *bifurcation of growth*, giving rise to the formation of the β-cylindritic crystalline superstructure.

Transcrystalline layers in iPP/fiber composites have been mainly investigated by polarized optical microscopy,[1,3−6,13−25,41] by far the most common and widespread method, SEM,[49] or AFM,[12,23,27] although there are some IR[22,42] and wide-angle X-ray diffraction studies;[27,50] in one case, X-ray microdiffraction using synchrotron radiation was used to study α-transcrystallinity induced by aramid fibers.[51] However, to our knowledge, there are no direct structural studies of the polymorphic interphase generated by pulling fibers through an iPP melt.

The ability to study the structure of the interphase region in fiber-reinforced composite materials with high spatial resolution is of particular interest, and a number of techniques can be considered. X-ray diffraction provides crystallographic information, and microdiffraction techniques can routinely probe areas from a few μm into the submicron range.[52] However, X-ray diffraction only provides information on the long-range order (crystalline) part of the polymer structures, and it is important to be able to complement this information with other techniques. Vibrational microspectroscopy can provide both local structural and chemical information at high spatial resolution. Thus, Raman spectroscopy can routinely achieve a lateral spatial resolution of 1−2 μm and has previously been used to study

* Corresponding author. E-mail: gary@ictp.csic.es.

10.1021/ma060760f CCC: $33.50
Published on Web 07/18/2006

interface effects in fiber-reinforced polymers,[53] including transcrystalline regions in polypropylene composites.[44,54,55] A logical development is therefore the combined use of synchrotron radiation microdiffraction and micro-Raman spectroscopy, which provides access to both local and long-range order information.[56] On the other hand, the spatial resolution of infrared microspectroscopy, defined by the numerical aperture of the microscope and the wavelength of the bands to be studied, has a practical limit of around 10 μm due to the limited IR intensity available through the energy-limiting apertures. However, synchrotron IR microspectroscopy overrides this limitation, providing a very bright diffraction-limited beam, and a spatial resolution of around $\lambda/2$ has been reported for confocal IR microscopes.[57]

Our main goal in this work was to obtain precise structural information of the fiber−matrix interphase by mapping regions of interest using both wide-angle X-ray microdiffraction and infrared microspectroscopy employing synchrotron radiation sources. We have focused our efforts on samples where fiber-pulling generates shear in the melt, investigating the nature of the crystalline interphase after crystallization is completed.

Experimental Section

Materials. A commercial grade isotactic polypropylene (REPSOL-YPF) was employed (isotacticity index = 95%, M_v = 164 700) and was characterized elsewhere.[58] The LCP fiber used was a wholly aromatic thermotropic main-chain liquid crystal copolyester, Vectra A950 167 TEX (Hoechst Ibérica), based on *p*-hydroxybenzoic acid (73 mol %) and 2,6-hydroxynaphthoic acid (27 mol %). Single filaments, around 23 μm in diameter, were carefully separated from the fiber bundles and sandwiched between two thin films of iPP and two microscope slides or a microscope slide and cover slip, which were then heated to 210 °C and held for 5 min in a Mettler FP80 or FP82 programmable hot stage. The temperature was then lowered to the isothermal crystallization temperature, and the fibers were manually pulled through the melt at a slow constant rate along the direction of the fiber axis.[30] After crystallization, the samples were cooled slowly to room temperature.

An overall sample thickness of around 60 μm was used for the X-ray measurements, whereas for transmission infrared microspectroscopy, to avoid saturation of the absobance, a sample thickness close to the fiber diameter was required.

Microfocus X-ray Diffraction. The X-ray diffraction experiments were carried out at the European Synchrotron Radiation Facility (ESRF) microfocus beam line (ID13) using a wavelength λ = 0.0948 nm (Si-111 monochromator) and a 3 μm diameter beam.[52] A two-dimensional CCD detector (MAR; 64.45 × 64.45 μm^2 pixels; 16 bit readout) was used to record the wide-angle X-ray patterns. The accumulation time was 30 s per step. The sample-to-detector signal distance was calibrated by an Ag-behenate sample as D = 175.6 mm.

The sample was aligned on a goniometer head so that the LCP fiber was almost horizontal. A specific point of the sample was selected by microscope and then transferred to the center of X-ray beam. The sample was scanned through the beam in 5 μm steps, with the fiber axis orthogonal to the X-ray beam. Data analysis was performed with the FIT2D software package.

Infrared Microspectroscopy. A Thermo Nicolet Continuμm Microscope, with a 50 μm detector area MCT detector, coupled to a Thermo Nicolet Magna 860 FTIR spectrometer, was employed at the U10B beamline of the National Synchrotron Light Source at Brookhaven National Laboratory, NY. The IR source is produced by the broadband synchrotron infrared radiation from a bending magnet. As such, a highly polarized and bright beam is available at the focal plane of the microscope.

The free-standing composite film was placed on the microscope stage, and crossed visible polarizers were used to locate the area of interest. Infrared spectra were collected at a spectral resolution of 4 cm^{-1} through an 8 μm confocal aperture at a data point step size of 8 μm using the Thermo Nicolet Atlμs IR mapping software.

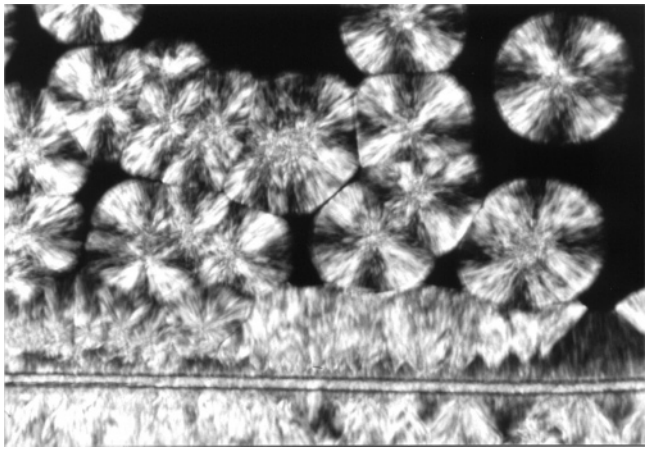

Figure 1. Crystalline superstructure formed by a Vectra A950 fiber on a iPP matrix during isothermal crystallization at 135 °C. The fiber was previously pulled at 140 °C.

Results and Discussion

Figure 1 presents polarized optical microphotographs of the morphology formed in iPP close to the position where an embedded LCP fiber has been pulled prior to isothermal crystallization at 135 °C. A complex interphase morphology can be observed, corresponding to a cylindritic β-phase in agreement with the literature. By far the most important evidence for the nature of these polymorphic interphases is provided by polarized thermooptical light microscopy[15,16,19,23,46]. Further, because the β-phase crystals of iPP melt at a lower temperature than the α-phase crystals, selective melting has demonstrated the persistence of a thin layer close to the fiber, which has been ascribed to α-phase crystals. This observation along with morphological data from SEM and AFM are the basis of the Varga and Karger-Kocsis model.[19]

The nature of the polymorphic interphase in an iPP/LCP fiber composite film, where the fiber was sheared at 140 °C and crystallized isothermally at 130 °C, was investigated by synchrotron IR microspectroscopy. Figure 2 shows an optical microphotograph obtained from an area of a free-standing film sample that contains a region around where the fiber was pulled, rich in different birrefringent structures, similar to those observed in Figure 1. A close up of the area studied and spectra obtained from the points indicated are given.

In previous work, subtle differences between the infrared spectra of α- and β-iPP have been identified and used to differentiate between the two crystalline forms.[59] Subsequent studies using synchrotron IR microspectroscopy has demonstrated that high spatial resolution polymorphic maps can be obtained.[30,59] Using the information from relative band intensities at specific sampling geometries in the highly polarized synchrotron IR beam, it is possible to differentiate between α-transcrystalline and β-cylindritic iPP.[30,60] Furthermore, the presence of a thin α-iPP layer close to the fiber in sheared iPP/LCP fiber composites was demonstrated, supporting earlier work using morphological and thermal techniques in other iPP/fiber composites.[23,61]

The spectra in Figure 2 correspond to α-, β-, and α-iPP, respectively, and correlate well with the polarized optical microscopy data, in that they also show a thin layer of α-phase iPP close to the fiber. The film was examined by point-by-point mapping in the area marked. The spectra were recorded through an 8 μm aperture with a step size of 8 μm, and the

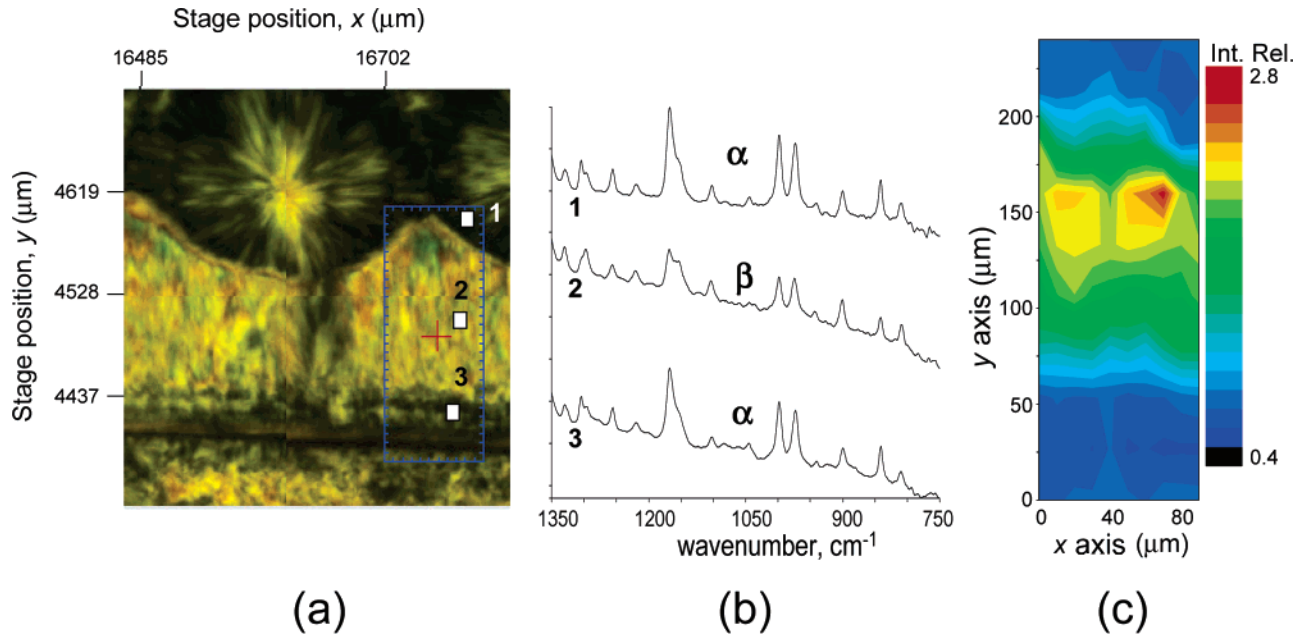

Figure 2. (a) Polarized optical microphotograph of a region of an isothermally crystallized film sample, showing points where IR spectra were recorded (numbered white boxes) and the mapped region (blue box), (b) spectra recorded at positions 1, 2, and 3, and (c) false color image of the marked region employing the 1296/1304 cm^{-1} intensity ratio.

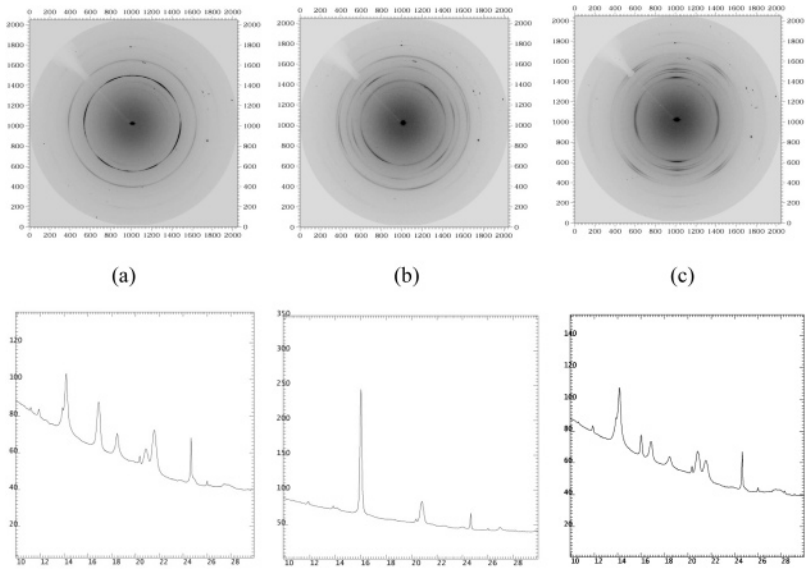

Figure 3. WAXS patterns of an iPP matrix crystallized under isothermal conditions at 135 °C in which a Vectra fiber was pulled out at 140°C. The sample was mapped from one side of the transcrystalline region to the other side with steps of 5 μm. (a) diffractogram corresponding to spherulite of α-crystalline form, (b) pattern showing reflections for β-cylindritic structure and (c) WAXS pattern recorded at the region that the fiber occupied.

resulting map measures 88 μm × 224 μm and contains 348 spectra. In Figure 2b, the spatial distribution of the different polymorphs is reflected by a false color contour image constructed using the 1296/1304 cm^{-1} band ratio, described previously.[30,60] In this map, we can clearly differentiate between α- and β-iPP, but we obtain no information from the fiber because the bands employed are not affected by the spectrum of the LCP fiber.

The synchrotron infrared microspectroscopy technique appears to provide solid evidence for the nature of the polymorphic interphases generated in iPP from shearing the LCP Vectra fiber. However, it should be noted that unequivocal identification of the different polymorphs by IR microspectroscopy depends on the relative orientation of the polymer chains with respect to the polarization axis of the synchrotron beam.[30]

For this reason, we have studied the same interphase structure employing wide-angle X-ray microdiffraction, scanning through the region of a sample where a Vectra fiber has been pulled out. The size of the microbeam, around 3 μm, is highly suited for analyzing the different regions of the sample, and particular attention was paid to the zones closest to the LCP fiber. A distance of around 200 μm from each side of the fiber was scanned in steps of 5 μm, and the diffractograms obtained from 3 different regions are shown in Figure 3.

The intensity of the WAXS patterns was radially integrated and the intensity profiles calculated and presented in Figure 4 as a function of the diffraction angle 2θ. A schematic representation of the different regions is given to the right of this figure. Since in this case the fiber has been completely removed from the sample, the shaded area corresponds with the position

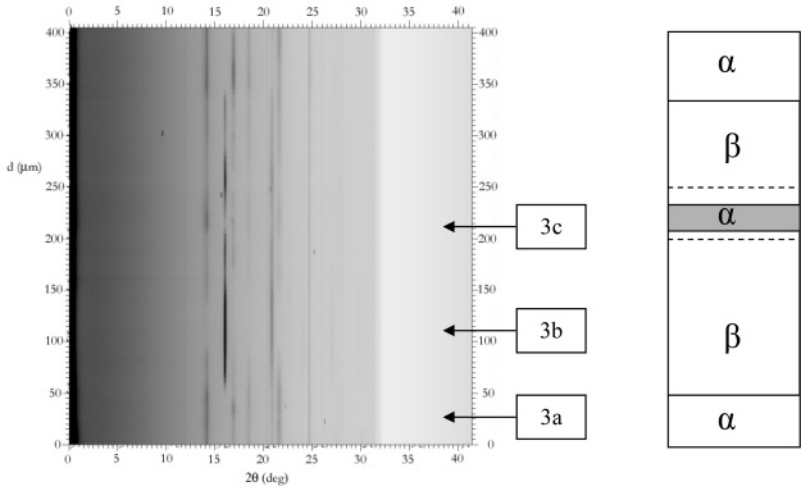

Figure 4. Integrated intensity of X-ray diffraction patterns at different 2θ angles for the diffractograms collected across the sample covering a large distance (d μm) from one side of fiber to the other. The sample is an iPP matrix crystallized under isothermal condition ns at 135 °C in which a Vectra fiber was pulled out at 140 °C. The positions corresponding to the diffractograms in Figure 3 are indicated.

initially occupied by the fiber. The discontinuous lines indicate the limit of the α-phase close to the position occupied by the fiber. From this figure, we can clearly observe that, in the region approximately corresponding to the first 60 μm, crystalline reflections corresponding to the α-form of iPP at $2\theta = 14°$, 17°, 18.5°, 21°, and 21.5° are clearly observed, as seen in Figure 3a. This region corresponds to the spherulitic region distant from the LCP fiber. From around 60 to 200 μm, the diffraction pattern corresponds to β-phase reflections at $2\theta = 16°$ and 21° and is associated with the cylindrical phase, Figure 3b. In the center of Figure 4, once again, reflections of the α-phase of iPP are observed and correspond with the iPP matrix close to the original position of the fiber, Figure 3c. In the diffractograms recorded on the other side of the fiber, an identical crystalline morphology hierarchy can be clearly observed.

These results unequivocally demonstrate the structure of the shear-induced cylindritic interphase, and confirms the model proposed by Varga and Karger-Kocsis.[19,61]

Conclusions

We have studied iPP matrixes with sheared LCP-fibers by thermooptical microscopy with polarized light, IR microspectroscopy, and X-ray microdiffraction employing synchrotron radiation sources. We have obtained spatially resolved crystallographic information for the first time from the polymorphic polymer−LCP fiber interphase region, which have allowed us to unequivocally relate spectroscopic and structural evidence to morphological details. The occurrence of a thin α-phase close a sheared fiber, which generates the cylindritic β-phase, has been clearly demonstrated by two structure-sensitive techniques.

The complimentarity of the synchrotron IR microspectroscopy and X-ray microdiffraction techniques in terms of sample preparation and spatial contrast provide a powerful method for the analysis of complex interphase behavior in reinforced polymer composites. The combined use of these techniques can be particularly important when studying the structure of semicrystalline polymer composites and alloys in general because IR provides information on chemical structure, conformation, and orientation and can be used to clearly define specific areas of interest in multiphase systems, whereas X-ray microdiffraction provides precise information on the crystallizable part of the material. Finally, because of the unique characteristics of the synchrotron IR beam, synchrotron IR microspectroscopy can be performed in an open laboratory environment, and sample optimization and measurement is quite versatile, facilitating the use of dual sampling strategies that allow microscopic samples to be studied in the same position in multiple techniques.

Recent developments[62,63] in high-temperature AFM imaging have provided clear discrimination between different types of α- and β-crystalline superstructures and may provide more insight into the polymorphic interphase region during its formation in fiber reinforced materials. It is our intention to pursue the study of this transition zone using high spatial resolution synchrotron microscopies in order to provide direct structural evidence.

Acknowledgment. Financial support is acknowledged from the Spanish Government in the projects MAT2002-03831 and MAT2002-04599. The infrared microscopy research was carried out at the National Synchrotron Light Source, Brookhaven National Laboratory, which is supported by the U.S. Department of Energy, Division of Materials Sciences and Division of Chemical Sciences, under contract no. DE-AC02-98CH10886. G.E. and P.D. wish to thank Dr. Lisa Miller and Dr. Larry Carr of the NSLS for useful discussions. We also thank Prof. Jerold M. Schultz for his helpful comments.

References and Notes

(1) Huson, M. G.; McGill, W. J. *J. Polym. Sci., Polym. Chem*. **1984**, *22*, 3571.
(2) Folkes, M. J. Interfacial Crystallization of Polypropylene in Composites. In *Polypropylene: Structure, Blends and Composites*; Karger-Kocsis, J., Ed.; Chapman & Hall: London, 1995; Vol. 3, p 340.
(3) Wang, C.; Hwang, L. M. *J. Polym. Sci., Part B: Polym. Phys.* **1996**, *34*, 1435.
(4) Wang, C.; Liu, C. R. *Polymer* **1999**, *40*, 289.
(5) Jenckel, E.; Teege, E.; Hinrichs, W. *Kolloid Z. Z Polym*. **1952**, *129*, 19−24.
(6) Quan, H.; Li, Z. M.; Yang, M. B.; Huang, R. *Compos. Sci. Technol.* **2005**, *65*, 999.
(7) Padden, F. J.; Keith, H. D. *J. Appl. Phys.* **1959**, *30*, 1479.
(8) Keith, H. D.; Padden, F. J.; Walter, N. M.; Wyckoff, H. W. *J. Appl. Phys.* **1959**, *30*, 1485.
(9) Natta, G.; Corradini, P. *Nuovo Cimento Suppl.* **1960**, *15*, 40.
(10) Turner-Jones, A.; Aizlewood, J. M.; Beckett, D. R. *Makromol. Chem.* **1964**, *75*, 134.
(11) Lotz, B.; Wittmann, J. C.; Lovinger, A. J. *Polymer* **1996**, *37*, 4979.
(12) Stocker, W.; Schumacher, M.; Graff, S.; Thierry, A.; Wittmann, J. C.; Lotz, B. *Macromolecules* **1998**, *31*, 807.
(13) Deveaux, E.; Chabert, B. *Polym. Commun.* **1991**, *32*, 464.
(14) Thomason, J. L.; Van Rooyen, A. A. *J. Mater. Sci.* **1992**, *27*, 907.
(15) Varga, J.; Karger-Kocsis, J. *Compos. Sci. Technol.* **1993**, *48*, 191.

CDV

(16) Varga, J.; Karger-Kocsis, J. *Polym. Bull.* **1993**, *30*, 105.
(17) Chabert, B.; Ouland Bouyahya Idrissi, M.; Guillet, J.; Nemoz, G. *Composites* **1984**, *5*, 49.
(18) Deveaux, E.; Chabert, B. *Polymer Commun.* **1990**, *31*, 391
(19) Varga, J.; Karger-Kocsis, J. *J. Polym. Sci., Part B: Polym. Phys.* **1996**, *34*, 657.
(20) Thomason, J. L.; Van Rooyen, A. A. *J. Mater. Sci.* **1992**, *27*, 889.
(21) Cai, Y.; Petermann, J.; Wittich, H. *J. Appl. Polym. Sci.* **1997**, *65*, 67.
(22) Wu, C.; Chen, M.; Karger-Kosics, J. *Polymer* **1999**, *40*, 4195.
(23) Vancso, G. J.; Liu, G.; Karger-Kocsis, J.; Varga, J. *Colloid Polym. Sci.* **1997**, *275*, 181.
(24) Bledzki, A. K.; Reihmane, S.; Gassan, J. *J. Appl. Polym. Sci.* **1996**, *59*, 1329.
(25) Mi, Y.; Chen, X.; Guo, Q. *J. Appl. Polym. Sci.* **1997**, *64*, 1267.
(26) Coutinho, F. M. B.; Costa, T. H. S.; Carvalho, D. L. *J. Appl. Polym. Sci.* **1997**, *65*, 1227.
(27) Wu, C.; Chen, M.; Karger-Kocsis, J. *Polymer* **2001**, *42*, 199.
(28) Tjong, S. C.; Liu, S. L.; Li, R. K. K. *J. Mater. Sci.* **1995**, *36*, 353.
(29) Jaffe, M. In *Encyclopaedia of Polymer and Engineering*, 2nd ed.; Mark, H. F., Bikales, N. M., Overberger, C. G., Menges, G., Eds.; Wiley & Sons: New York, 1987; Vol. 7.
(30) Ellis, G.; Marco, C.; Gómez, M. A. *J. Macromol. Sci., Phys.* **2004**, *B43*, 191.
(31) Karger-Kocsis, J. *Polym. Eng. Sci.* **1996**, *36*, 203.
(32) Karger-Kocsis, J.; Moos, E.; Mudra, I.; Varga, J. *J. Macromol. Sci., Part B: Phys.* **1999**, *38*, 645.
(33) Tordjeman, Ph.; Robert, C.; Marin, G.; Gerard, P. *Eur. Phys. J.* **2001**, *E4*, 459.
(34) Varga J. *J. Macromol. Sci., Phys.* **2002**, *41*, 1121.
(35) Lovinger, A. J.; Chua, J. O.; Gryte, C. C. *J. Polym. Sci., Polym. Phys. Ed.* **1977**, *15*, 641.
(36) Zipper, P.; Janosi, A.; Wrentschur, E.; Abuja, P. M.; Knabl, C. *Prog. Colloid Polym. Sci.* **1993**, *93*, 377.
(37) Leugering, H. J. *Makromol. Chem.* **1967**, *109*, 204.
(38) Varga, J. *J. Therm. Anal.* **1986**, *31*, 165.
(39) Varga, J.; Mudra, I.; Ehrenstein, G. W. *J. Appl. Polym. Sci.* **1999**, *74*, 2357.
(40) Li, J. X.; Cheung, W. L. *Polymer* **1999**, *40*, 2085.
(41) Varga, J. Crystallization, Melting and Supermolecular Structure of Isotactic Polypropylene. In *Polypropylene. Structure, Blends and Composites, Vol. 1: Structure and Morphology*; Karger-Kocsis, J. Ed.; Chapman & Hall: London, 1995; Vol. 1, pp 56−115.
(42) Lustiger, A.; Marzinsky, C. N.; Mueller, R. R.; Wagner, H. D. *J. Adhes.* **1995**, *53*, 1.
(43) Assouline, E.; Pohl, S.; Fulchiron, R.; Gerard, J.-F.; Lustiger, A.; Wagner, H. D.; Marom, G. *Polymer* **2000**, *41*, 7843.
(44) Fernandez, M. R.; Merino, J. C.; Gobernado-Mitre, M. I.; Pastor, J. M. *Appl. Spectrosc.* **2000**, *54*, 1105.
(45) Li, H.; Zhang, X.; Duan, Y.; Wang, D.; Li, L.; Yan, S. *Polymer* **2004**, *45*, 8059.
(46) Sun, X.; Li, H.; Zhang, X.; Wang, J.; Wang, D.; Yan, S. *Macromolecules* **2006**, *39*, 1087.
(47) Varga, J.; Karger-Kocsis, J. *Mater. Sci. Lett.* **1994**, *13*, 1069.
(48) Zhang, C.; Hu, H.; Wang, D.; Yan, S.; Han, C. C. *Polymer* **2006**, *46*, 8157.
(49) Loos, J.; Schimanki, T.; Hofman, J.; Peijs, T.; Lemstra, P. J. *Polymer* **2001**, *42*, 3827.
(50) Dean, D. M.; Rebenfeld, L.; Register, R. A.; Hsiao, B. S. *J. Mater. Sci.* **1998**, *33*, 4797.
(51) Assouline, E.; Watchel, E.; Grugull, S.; Lustiger, A.; Wagner, H. D.; Marom, G. *Polymer* **2001**, *42*, 6231.
(52) Riekel, C.; Davies, R. *Curr. Opin. Colloid Interface Sci.* **2005**, *9*, 396.
(53) Young, R. J. *Key. Eng. Mater.* **1996**, *116−117*, 173.
(54) Heppenstall-Butler, M.; Bannister, D. J.; Young, R. J. *Composites, Part A* **1996**, *27*, 833.
(55) Nielsen, A. S.; Pyrz, R. *J. Mater. Sci.* **2003**, *38*, 597.
(56) Davies, R.; Burghammer, M.; Riekel, C. *Appl. Phys. Lett.* **2005**, *87*, 264105
(57) Carr, G. L. *Rev. Sci. Instrum.* **2001**, *72*, 1613.
(58) Marco, C.; Gómez, M. A.; Ellis, G.; Arribas, J. M. *J. Appl. Polym. Sci.* **2002**, *84*, 1669.
(59) Ellis, G.; Marco, C.; Gómez, M. A. *Int. J. Vib. Spectrosc.* **2001**, *5* (4), 7, www.ijvs.com.
(60) Ellis, G.; Marco, C.; Gómez, M. A. *Infrared Phys. Technol.* **2004**, *45*, 349.
(61) Varga, J.; Karger-Kocsis, J. *Polymer* **1995**, *36*, 4877.
(62) Zhou, J. J.; Liu, J. G.; Yan, S. K.; Dong, J. Y.; Li, L.; Cham, C. M.; Schultz, J. M. *Polymer* **2005**, *46*, 4077.
(63) Zhou, J. J.; Li, L.; Lu, J. *Polymer* **2006**, *47*, 261.

MA060760F